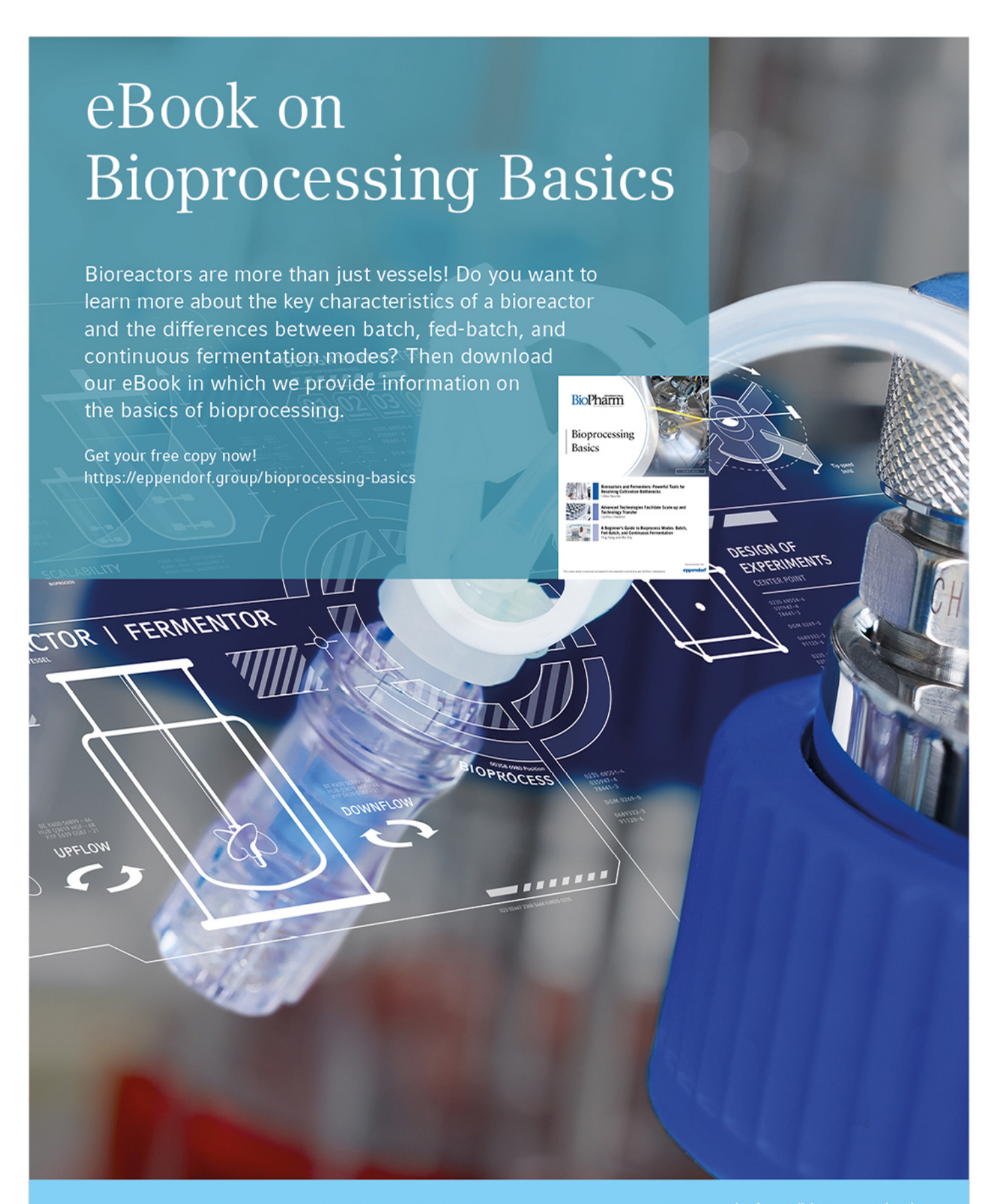
eppendorf



0970290, 0, Downloaded from https://onlinelibrary.wiley.com/doi/10.1002/bit.28319 by Cornell University, Wiley Online Library on [26/01/2023]. See the Terms and Conditions (https://onlinelibrary.wiley.com/terms-and-conditions) on Wiley Online Library for rules of use; OA articles are governed by the applicable Creative Commons Licensean Conditions (https://onlinelibrary.wiley.com/terms-and-conditions) on Wiley Online Library for rules of use; OA articles are governed by the applicable Creative Commons Licensean Conditions (https://onlinelibrary.wiley.com/terms-and-conditions) on Wiley Online Library for rules of use; OA articles are governed by the applicable Creative Commons Licensean Conditions (https://onlinelibrary.wiley.com/terms-and-conditions) on Wiley Online Library for rules of use; OA articles are governed by the applicable Creative Commons Licensean Conditions (https://onlinelibrary.wiley.com/terms-and-conditions) on Wiley Online Library for rules of use; OA articles are governed by the applicable Creative Commons Licensean Conditions (https://onlinelibrary.wiley.com/terms-and-conditions) on Wiley Online Library for rules of use; OA articles are governed by the applicable Creative Commons Licensean Conditions (https://onlinelibrary.wiley.com/terms-and-conditions) on Wiley Online Library for rules of use; OA articles are governed by the applicable Creative Commons (https://onlinelibrary.wiley.com/terms-and-conditions) on the applicable Creative Commons (https://onlinelibr

DOI: 10.1002/bit.28319

ARTICLE



A high-throughput expression and screening platform for applications-driven PETase engineering

Hannah S. Zurier D | Julie M. Goddard D

Department of Food Science and Technology, Cornell University, Ithaca, New York, USA

Correspondence

Julie M. Goddard, Department of Food Science and Technology, Cornell University, 365 Stocking Hall, Ithaca, New York 14853, USA. Email: goddard@cornell.edu

Funding information

U.S. Department of Agriculture

Abstract

The environmental consequences of plastic waste have impacted all kingdoms of life in terrestrial and aquatic ecosystems. However, as the burden of plastic pollution has increased, microbes have evolved to utilize anthropogenic polymers as nutrient sources. Of depolymerase enzymes, the best characterized is PETase, which hydrolyzes aromatic polyesters. PETase engineering has made impressive progress in recent years; however, further optimization of engineered PETase toward industrial application has been limited by lower throughput techniques used in protein purification and activity detection. Here, we address these deficiencies through development of a higher-throughput PETase engineering platform. Secretory expression via YebF tagging eliminates lysis and purification steps, facilitating production of large mutant libraries. Fluorescent detection of degradation products permits rapid screening of depolymerase activity in microplates as opposed to serial chromatographic methods. This approach enabled development of more stable PETase, semi-rational (SR) PETase variant containing previously unpublished mutations. SR-PETase releases 1.9-fold more degradation products and has up to 7.4-fold higher activity than wild-type PETase over 10 days at 40°C. These methods can be adapted to a variety of chemical environments, enabling screening of PETase mutants in applications-relevant conditions. Overall, this work promises to facilitate advancements in PETase engineering toward industrial depolymerization of plastic waste.

KEYWORDS

enzyme engineering, high-throughput screening, microplastics, PETase, plastic degradation, semi-rational design

INTRODUCTION

A total of 300 million tons of plastic are discarded every year, resulting in an environmental accumulation of over 5 billion tons of plastic waste material since 1950. Much of this waste is in the form of microplastics: particles and fibers no more than 5 mm in their longest dimension. Microplastics are a ubiquitous pollutant in both terrestrial and aquatic environments and have been linked to acute and chronic toxicity in animals, plants, and microbes. When present in agricultural settings, microplastics can reduce crop yields and damage the native microbial consortia that maintain the nutrient balance of soils (De Souza MacHado et al., 2018, 2019; Seeley et al., 2020). In

addition to the inherent toxicity of microplastics, their hydrophobicity enables adsorption of toxic small molecules, creating poison sinks that can cause further damage to organisms and ecosystems (Godoy et al., 2019; Wong et al., 2020). Half-lives of common plastic materials range from years to millennia (Geyer et al., 2017) and it is estimated that nearly all plastic ever manufactured persists in some form in the environment (Geyer et al., 2017), making microplastics a chronic, persistent pollutant.

Microplastics resist degradation due to the same properties that make plastic materials so useful: inert surface chemistry and inherent durability (K. Zhang et al., 2021). However, their small size and correspondingly large surface area per unit mass permit more

efficient depolymerization than larger plastic substrates; thus, a range of physical (Uheida et al., 2021), chemical (Ariza-Tarazona et al., 2020; Zhou et al., 2021), and biological (Gong et al., 2018; Shabbir et al., 2020; Zhou et al., 2021) means have been explored to enhance microplastic degradation. Biocatalytic depolymerization represents a particularly exciting approach due to its potential for green, in situ degradation (Zurier & Goddard, 2021). Previous research has identified microbes and microbial consortia with depolymerization activity, with substrates encompassing the much of the chemical breadth of commodity plastics, including aliphatic (Hadad et al., 2005; Yang et al., 2021) and aromatic (Ho et al., 2017) hydrocarbon polymers, polyurethanes (Loredo-Treviño et al., 2012), and polyesters (Yoshida et al., 2016). One of the first identified, and to date best characterized, depolymerase enzymes isolated from a plastic-degrading microbe is the poly (ethylene) terephthalate (PET) hydrolase native to Ideonella sakaiensis, an organism first isolated by Yoshida et al. from a recycling center in Japan (Yoshida et al., 2016). This enzyme, termed PETase, has generated much interest for its potential to reduce the environmental burden of microplastic pollution (Koshti et al., 2018). PETase directly converts insoluble PET to soluble monomers of mono-2-hydroxyethyl terephthalate (MHET) (Yoshida et al., 2016), meaning that this enzyme has the potential to enable facile, one-pot biodegradation on an industrial scale if limitations on its native efficiency and stability under industrial catalysis applications could be overcome. (Joo et al., 2018).

Engineering of enzymes at the amino acid level can significantly increase reaction velocity and catalytic stability in process-relevant conditions which are often denaturing (Woodley, 2013). Much biochemical and structural characterization has revealed key molecular features of PETase (Austin et al., 2018; Bååth et al., 2021; Chen et al., 2018; Joo et al., 2018; Liu et al., 2018), enabling more targeted and efficient applications of engineering principles. Strategies such as rational design, in which evolutionary, structural, and mechanistic information are used to identify key mutations, and semi-rational engineering, which involves computational identification of a library of potentially beneficial mutations, have been employed to develop new PETase variants (Austin et al., 2018; Cui et al., 2021; Lu et al., 2022; Ma et al., 2018; Son et al., 2019, 2020). The goal of these studies has been to increase PETase activity and melting temperature relative to wild type in chemically defined, buffered conditions. Successful variants include DuraPETase, whose 10 individual point mutations confer a 300-fold increase in activity and 31°C increase in melting temperature relative to wild-type PETase (Cui et al., 2021), FastPETase, with six single point mutations and a 29-fold increase in activity relative to wildtype (Lu et al., 2022), and ThermoPETase, with three point mutations, an 8.81°C increase in melting temperature and 14-fold increase in activity relative to wild-type (Son et al., 2019). These improvements are significant; however, to date all published expression and screening techniques used to produce these highly active mutants are laborintensive, limiting capacity for further engineering toward industrial applicability. There is thus a need to overcome the technical limitations of the existing state-of-the-art in PETase expression and screening methodology that hinder throughput.

In this study, we present a high-throughput PETase engineering platform using secretory expression and fluorescent product detection that aims to promote facile transition of successful variants toward industrial applications. Secretory production of PETase mutants eliminates purification steps, while fluorescent detection of degradation products enables high-throughput screening in microplates, cutting down processing times from minutes per sample, run serially, to under a minute for 96 samples run near-simultaneously. This approach has enabled us to develop a new PETase variant, SR-PETase, containing previously unpublished mutations with significantly higher sustained activity than the wild-type enzyme. While it is challenging to compare this mutant to published data due to the novelty of the methods used for expression and detection, we did find between 1.9 and 7.4-fold higher activity than wild-type PETase at 40°C over a 10 day period. This activity increase is in line with the gains made by published mutants in similar conditions. Beyond the scope of this highly active mutant, the high-throughput engineering platform presented herein could be used to develop a PETase mutant for targeted applications across a range of process conditions, thus expanding the potential for PET depolymerization to be integrated into a wide range of systems.

2 | MATERIALS AND METHODS

2.1 | Materials

All reagents were purchased from Sigma-Aldrich unless otherwise noted. Mono-hydroxyethyl terephthalate was purchased from Advanced Chemblocks Inc. under the name 4- (2-hydroxyethoxy) carbonyl)benzoic acid. 1/8" 10 dpf (Denier Per Filament), (3.2 mm long, 32 μm diameter, T_g 90.4 \pm 3.6°C, T_m 253.8 \pm 1.1°C, 20.5 \pm 1.2% crystallinity, 1.38 g/cm³ density) precision cut PET microfibers were provided as a free sample from MiniFIBERS In. Density of PET microfibers was calculated based on the manufacturer's provided equation below:

Diameter (mm) =
$$11.89x \sqrt{\frac{dpf}{density(\frac{g}{cm^3})}}$$
.

Custom DNA oligonucleotides and genes were synthesized by Integrated DNA Technologies (IDT).

2.2 | Mutant library design

The IsPETase sequence (UniProt A0A0K8P6T7) and structure (PDB 5XJH) were submitted to the HotSpot Wizard (Sumbalova et al., 2018), FireProt (Musil et al., 2017), and PROSS (Goldenzweig et al., 2016) servers. Outputs were manually correlated to identify positions where mutagenesis would likely be functionally tolerated and residues that would offer enhanced structural stability. Mutations that were identified by multiple algorithms and indicated to

have moderate or high mutability by HotSpot Wizard were selected for further study. The pared down list of positions was checked by annotating the structure in PyMol (Schrodinger LLC, 2021) to ensure a broad structural distribution of mutations. This process was iterated to afford a library of 57 single point mutations, of which 54 are new to this study.

2.3 | Cloning

Expression plasmid pNRG-0186 was constructed from the pET 11a backbone (Invitrogen) using HiFi DNA assembly (NEB). YebF was amplified from a plasmid provided by the DeLisa lab (Cornell University) by polymerase chain reaction (PCR) with the primers in Supporting Information: Table S1 using Q5 HotStart 2X PCR Master Mix (NEB). pET 11a was linearized by PCR with using Q5 HotStart 2X PCR Master Mix and primers in Supporting Information: Table S1. Amplification was verified by agarose gel electrophoresis. Template DNA was degraded by incubation of PCR reactions with DpnI restriction enzyme (NEB). Amplicons were then purified using the Nucleospin PCR Clean Up Kit (Macherey-Nagel). PETase was synthesized as a codon-optimized custom gene fragment by IDT. Purified DNA was combined at a 3:3:1 yebF:PETase:linearized pET 11a molar ratio with NEBuilder® HiFi DNA Assembly Master Mix (NEB) and incubated for 1 h at 50°C. Assembled plasmids were electroporated into E. cloni® 10G Electrocompetent Cells (Lucigen) and plated on LB-agar supplemented with 100 µg/ml ampicillin (LB-Amp). Colonies were amplified in liquid culture and DNA was purified with the QIAprep Spin Miniprep Kit (Qiagen). Successful assembly was validated by Sanger DNA sequencing at the Cornell Biotechnology Resources Center. A similar method was used to produce YebF-tagged mutants with a C-terminal hexahistidine tag (pNRG-0187), using primers from Supporting Information: Table S1. To create pPETase, a construct with WT PETase and no YebF tag or native signal peptide (pNRG-0188), a similar method was used, using primers from Supporting Information: Table S1. Mutants were produced using the QuikChange method of site-directed mutagenesis (Agilent Technologies Inc) using the primers in Supporting Information: Table S2 and PfuUltra II Hotstart PCR Master Mix (Agilent). Plasmids were transformed into High Efficiency NEB® 5-alpha Competent Escherichia coli and plated on LB supplemented with 100 µg/ml ampicillin (LB-Amp). Colonies were amplified in LB-Amp and plasmids purified with the QIAprep Spin Miniprep Kit (Qiagen) before validation by Sanger DNA sequencing at the Cornell Biotechnology Resources Center.

2.4 | Differential scanning calorimetry

PET fibers were analyzed using a TA Instruments Differential Scanning Calorimetry (DSC) Auto 2500 Differential Scanning Calorimeter (Waters) located in the Cornell Center for Materials Research. Samples were equilibrated at 0°C, heated at a rate of

10°C/min to 300°C, held at 300°C for 1 min, and cooled at a rate of 10°C/minute to 0°C. Percentage crystallinity was determined using the following formula:

%crystallinity =
$$\frac{\triangle H_m - \triangle H_{cc}}{\triangle H_m^{\circ}} \times 100$$
,

where $\triangle H_m$ is the heat of fusion, $\triangle H_{cc}$ is the heat of cold crystallization, and $\triangle H_m^{\circ}$ is the heat of fusion for 100% crystalline PET. To determine $\triangle H_m$ and $\triangle H_{cc}$, the area under the DSC curve was integrated using the TRIOS software package (Waters). The reference value used for $\triangle H_m^{\circ}$ was 140.1 J/g (Son et al., 2019). Glass transition temperature and melting temperature were also determined using TRIOS. All values determined by DSC are presented in Supporting Information: Table S3.

2.5 | PETase mutant secretory expression

pNRG-0186, pNRG-0187, pNRG-0188, and all mutants thereof were transformed into BL21 (DE3) *E. coli* for expression. Overnight cultures were grown from single colonies in LB-Amp at 37°C with 200 RPM shaking. ZYM-5052 auto-induction media (Studier, 2005) supplemented with 100 μ g/ml ampicillin was inoculated with 1% volume of overnight culture and incubated at 37°C with 200 RPM shaking for 4 h. Cultures were then moved to 20°C and expression continued for 20–22 h with constant shaking at 200 RPM. Cells were pelleted by centrifugation (2000g, 10 min) and supernatants were used immediately for further experiments. To facilitate these high-throughput experiments, cultures were grown in 1 ml volumes in 96-well Deepwell plates (Eppendorf).

2.6 | PETase cytosolic expression and lysis

To compare cytosolic and secretory expression, pNRG-0186 and pNRG-0188 were transformed into BL21 (DE3) *E. coli* for expression. Overnight cultures were grown from single colonies in LB-Amp at 37°C with 200 RPM shaking. ZYM-5052 supplemented with $100\,\mu\text{g/ml}$ ampicillin was inoculated with 1% volume of overnight culture and incubated at 37°C with 200 RPM shaking for $4\,\text{h}$. Cultures were then moved to 20°C and expression continued for $20\text{--}22\,\text{h}$ with constant shaking at $200\,\text{RPM}$. Cells were pelleted by centrifugation (2000g, $10\,$ min). Pellets were lysed with $5\,\text{ml/gram}$ Bacterial Protein Extraction Reagent (B-PER Complete, Thermo Fisher Scientific) for $15\,\text{min}$ at 20°C . Lysates were diluted five-fold with sterile ZYM-5052 medium pelleting cell debris by centrifugation (3260g, $1\,\text{h}$). Clarified lysates and supernatants were used immediately for comparative degradation studies.

2.7 | PETase activity measurement

To create standard curves, terephthalic acid (TPA), MHET, and bishydroxyethyl terephthalic acid (BHET) were dissolved in reaction



buffer (50 mM glycine-NaOH, pH 8.5) at the required concentrations. A total of 200 μ l samples were added to the wells of a black 96-well microplate (Corning Inc) containing 20 μ l/well of 50 mM FeSO₄ + 500 mM EDTA, pH 8.5. Plates were covered in foil and incubated, shaking 90 RPM for 25 min. Fluorescence (ex. 328/20 nm, em. 421/20 nm) was read using a UV/vis fluorescence spectrophotometer (Synergy Neo 2, BioTek). Curves were fitted using liner regression in GraphPad Prism 7.

To measure degradation activity, single PET microfibers were added to wells of 96-well optically clear polystyrene microplates (Porvair) with static-free tweezers (Antylia Scientific). A total of 200 µl supernatant from PETase expression was added to each well and plates were incubated without rotation at 20°C for 1 h to allow PETase to bind to PET fibers. Supernatant was then aspirated from wells and replaced with 200 µl reaction buffer. Plates were sealed with Microplate Sealing Tape (Thermo Fisher Scientific) and incubated without rotation at 40°C for up to 72 h of reaction time, with contents of wells aspirated and analyzed for kinetic parameters at regular intervals (16, 24, 40, 44, 48, 52, 64, 68, 72 h). In initial screening experiments, activity was measured at single time point of 72 h reaction time. Upon removal, supernatants were added to black 96-well plates containing 20 µl/well of 50 mM FeSO4 + 500 mM EDTA, pH 8.5. Plates were covered in foil and incubated, shaking 90 RPM for 25 min. Fluorescence (ex. 328 nm, em. 421 nm) was read at the using the BioTek spectrophotometer.

2.8 | PETase purification

HisPur cobalt resin (Thermo Fisher Scientific) was equilibrated in dilution buffer (reaction buffer containing 300 mM NaCl). Hexahistidine tagged mutants were expressed as described. Supernatants from expression cultures of pNRG-0187 and mutants thereof were concentrated 100-fold in 10 kDa MWCO centrifugal filtration membranes (MilliporeSigma). Concentrated supernatants were diluted 25-fold in dilution buffer and incubated at 16°C for 45 min with rotation at 32 RPM. Resin was pelleted by centrifugation (700g, 2 min), after which supernatant was aspirated and discarded. To remove nonspecifically bound proteins, resin was washed with 1 ml dilution buffer and pelleted again. The wash step was then repeated with dilution buffer supplemented with 10 mM imidazole. Protein was eluted in three subsequent stages by washing the resin with 250 µl dilution buffer supplemented with 25, 50, and 100 mM imidazole, respectively. Elutions were pooled and concentrated to 100 µl using 10 kDa MWCO centrifugal filter membranes. Concentrates were diluted five-fold with reaction buffer and dilutions were concentrated again to 100 µl. This process was repeated a total of three times to exchange the eluted protein into reaction buffer and the volume of the final product was normalized to 200 µl with reaction buffer. Purified protein was quantified using the bicinchoninic acid assay (Thermo Fisher Scientific). Samples containing more than 65 µg/ml (2.5 µM) protein were used immediately for Differential Scanning Fluorimetry (DSF) experiments.

2.9 | DSF

Single PET microfibers were added to half the wells of 96-well MicroAmp™ Optical 96-well Reaction Plates (Thermo Fisher Scientific) with static-free tweezers. 20 µl purified protein was mixed with 30 µl reaction buffer and 50 nl SYPRO™ Orange Protein Gel Stain for a total concentration of 5X stain. Plates were sealed with MicroAmp™ Optical Adhesive Film (Thermo Fisher Scientific) and covered in aluminum foil until analysis. Differential scanning fluorimetry was performed within 15 min of adding dye to samples in a QuantStudio 6 Flex Real-Time PCR machine (Thermo Fisher Scientific) located in the Wiedmann Lab (Cornell University) using the method described by Huynh and Partch (Huynh & Partch, 2015). In brief, samples were held at 25°C for 2 min and temperature was ramped stepwise by 1°C followed by a 1-min incubation at this increased temperature before the next ramp. Once the temperature reached 95°C, the samples were held for 2 min before conclusion of the experiment. Fluorescence was read at 1-min intervals using the ROX laser (ex. 586 nm, em. 605 nm). Data was fitted to sigmoidal models using the DSF world server (Wu et al., 2020). Melting points were defined as the inflection point on the sigmoidal fit (Wu et al., 2020).

2.10 | Statistical analysis

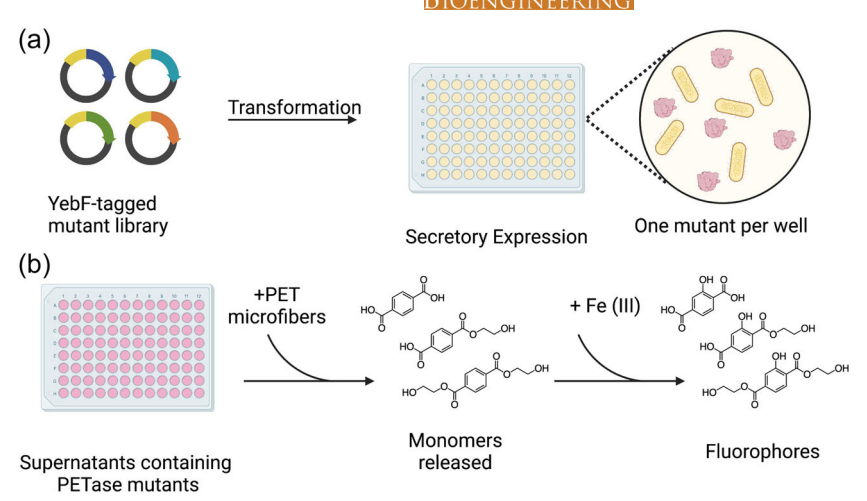
Statistical analyses were all performed in GraphPad Prism 7. All experiments were performed with 3–4 technical replicates. Data are presented as representative of at least two biological replicates. Specific statistical tests used are noted in relevant figure legends. Significance was determined with a cutoff of $\alpha \le 0.05$.

3 | RESULTS AND DISCUSSION

3.1 | Design of high-throughput PETase mutagenesis platform

Throughput of mutant screens remains the major bottleneck in protein engineering by semi-rational and directed evolutionary means (Zeng et al., 2020). Elimination and near-parallelization of labor-intensive experimental processes enables higher throughput. PETase engineering efforts have been limited in throughput by two primary methodological variables: protein expression system and product detection strategy (Cui et al., 2021; Lu et al., 2022; Pirillo et al., 2021; Son et al., 2019). Our platform overcomes these limitations through secretory expression (G. Zhang et al., 2006), which eliminates laborious lysis and purification steps, and fluorescent product detection (Ebersbach et al., 2012), which near-parallelizes what is traditionally accomplished by liquid chromatography (Figure 1).

Previously published studies have expressed PETase as a cytosolic protein, requiring lysis and purification procedures before activity can be measured (Cui et al., 2021; Lu et al., 2022; Son et al., 2019). While



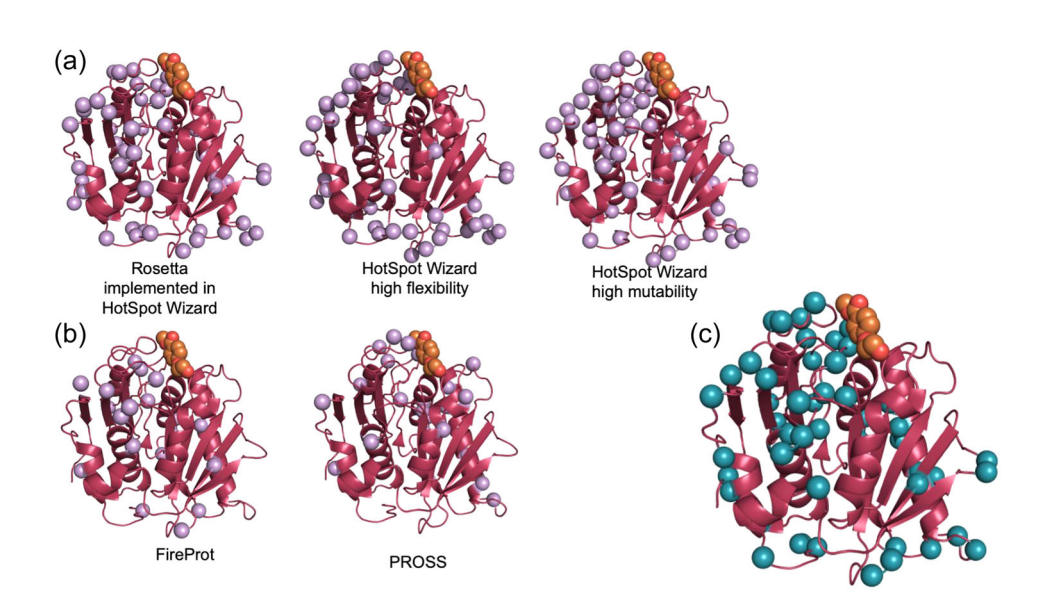


FIGURE 2 Semi-rational design of PETase mutant library. PETase is shown in all images as rose-colored cartoon. Mutant sites are shown as highlighted spheres at alpha carbon. Mono-2-hydroxyethyl terephthalate is shown in orange spheres to give perspective on the location of the active site. All images are derived from 5XJH in the protein data bank. (a) Mutant sites identified by different algorithms of the HotSpot Wizard webserver. From left to right, sites shown were identified as beneficial by Rosetta implemented in HotSpot Wizard, in highly flexible sites identified by the HotSpot Wizard algorithm, and highly mutable sites identified by the HotSpot Wizard algorithm. (b) Mutant sites identified by FireProt and PROSS algorithms. For (a) and (b), mutation sites are highlighted in lavender, and algorithms were fed information from structure 5XJH from the protein data bank and sequence A0A0K8P6T7 from the UniProt database. (c) Mutant sites selected for experimental screening. Mutation sites are highlighted in teal.

secretory expression has been used to produce extracellular PETase (Huang et al., 2018; Lu et al., 2022; Seo et al., 2019; Shi et al., 2021), this technique has not yet been applied in high-throughput engineering studies. Since secretory expression increases throughput by reducing the number of experimental processes required to screen mutant proteins, we built our engineering platform around extracellular protein production. N-terminal YebF fusion (G. Zhang et al., 2006) was used to target PETase for excretion (Supporting Information: Figure S1A), which resulted in >80% of total enzymatic activity present in the expression media (Supporting Information: Figure S1B). PETase without a YebF fusion tag had <30% of total enzymatic activity present

in the expression media, with the balance in the clarified cell lysate (Figure 2b). In this work, we chose not to normalize protein concentration between wells, both to further streamline screening and because secretion kinetics are another important factor in the eventual application of the engineered protein whose ultimate goal is increased PET degradation. Cultures were grown in 1 ml volumes in 96 deep well plates to facilitate parallel analyses. To overcome the bottleneck in product detection imposed by chromatography, we leveraged spectroscopic techniques that enable near-simultaneous processing of samples in microplates (Ebersbach et al., 2012) (Figure 1b). Both absorbance and fluorescent spectroscopy have been

shown to quantitatively detect PETase degradation products (Ebersbach et al., 2012; Pirillo et al., 2021; Zhong-Johnson et al., 2021), with similar sensitivity and dynamic range to chromatographic methods. We selected fluorescence of oxidized degradation products (oxidized bis- (2-hydroxyethyl) terephthalate (BHET-OH), mono- (2-hydroxyethyl) terephthalate (MHET-OH), and terephthalic acid (TPA-OH)) to quantify PETase activity as this technique performs in a wide range of reaction conditions typical of end-use applications but incompatible with absorbance (e.g., solutions that are not optically clear, presence of aromatic compounds, etc). Combined, the use of secretory expression and fluorescent detection enabled rapid screening of PETase mutants for degradation activity.

In this work, we use PET microfibers as the model substrate for our degradation platform, a departure from the PET films used in previous studies (Cui et al., 2021; Lu et al., 2022; Son et al., 2019; Zhong-Johnson et al., 2021). While PET films are an excellent substrate for studies whose target end use application is in PET upcycling (e.g., recovery of degradation products for repolymerization or conversion into value-added chemicals), our interest is in eventual application of PETase to degrade microplastics in wastewater, a significant environmental burden (Zurier & Goddard, 2021). In addition to a focus on microplastics degradation, most PET manufactured globally is used for textiles (Kumartasli & Avinc, 2020), thus, our study focuses on degradation of microfibers by PETase. The microfibers had $20.5 \pm 1.2\%$ crystallinity, a melting temperature of $253.8 \pm 1.1^{\circ}$ C, and a glass transition temperature of $90.4 \pm 3.6^{\circ}$ C (Supporting Information: Table S3)

3.2 | Semi-rational design of PETase mutant library

To test our high-throughput PETase engineering platform, we built a library of 57 single point mutations with predicted stabilizing and/or activity-enhancing effects using a semi-rational strategy. Because PETase is well-characterized structurally and biochemically (Austin et al., 2018; Chen et al., 2018; Fecker et al., 2018; Joo et al., 2018), we were able to guide our library design toward mutations that were most likely to be beneficial. Since there are many possible ways to predict protein mutagenesis sites, all of which make various assumptions about the biochemical effects of mutagenesis, we aimed to minimize bias in library design by using multiple prediction algorithms (HotSpot Wizard [Sumbalova et al., 2018], Rosetta [Sumbalova et al., 2018], FireProt [Musil et al., 2017], PROSS [Goldenzweig et al., 2016]) and comparing the results (Figure 2, Table 1, Supporting Information: Table S4).

We found that while different prediction algorithms rely on different assumptions, patterns emerged in their outputs when fed the PETase structure and sequence. For example, the loops directly opposite the active site were highlighted by multiple algorithms as being both highly flexible and poorly conserved, indicating that their mutagenesis would likely increase stability while sparing activity. The total output of the algorithms is shown in Supporting Information: Table S4 chosen mutants and the algorithms that selected them are catalogued in Table 1. We then

selected mutants based on correlations between the different algorithms to pursue experimentally. Overall, of the mutants screened, 54 (95%) are new to this study, highlighting the novelty of this approach in the PETase engineering field.

3.3 | Initial screens reveal a subset of highly active PETase mutants

We screened the selected library of mutants in high throughput using the expression and detection techniques described in Figure 1 and the methods section (Supporting Information). Two negative controls were used in this analysis and in subsequent analyses of mutant activity. "Dead," a PETase variant in which active site residues were mutated to alanines (S160A/D206A/H237A) was a PETase mutant with no possible depolymerase activity. "Blank" was a PET fiber incubated without any PETase present. Screening of mutant activity on single PET microfibers in individual microplate wells revealed that after 72 h of incubation, some mutants had significantly more PETase degradation products released than wild type PETase. In particular, a subset of 12 single point mutants had significantly higher PETase activity across multiple biological replicates than the wild-type enzyme across multiple biological replicates (Figure 3a). Analysis of these mutants in the context of the PETase structure (Supporting Information: Figure S2) showed their improved performance is likely due to formation of new intramolecular interactions that enhance overall stability. This pared down library of 12 mutants was then combined as double mutants for further screening and analysis.

3.4 | Combining high-performing mutations produces synergistic effects

We combined the 12 mutants identified by initial screens into 57 double mutants and repeated the screening process (Figure 4a). Interestingly, while some double mutants had lower overall activity than their parent single mutants, most had higher activity. Overall, nine double mutants had synergistic benefits, which we defined as significantly (p < 0.05) higher activity than both parent mutants. In addition to the higher concentration of products released, these nine selected double mutants also had significantly higher melting temperatures (T_m) than their parent mutants (Figure 4b), indicating that increased thermostability helped drive this increase in overall activity. This increase in T_m is consistent in both the presence and absence of PET substrate (Figure 4b, Supporting Information: Figure S3). Because the presence of PET does not have a stronger stabilizing influence on mutants than on WT PETase, we hypothesize that the increase in activity displayed by the mutant enzymes is not driven by increased substrate affinity. This hypothesis is consistent with the observation that mutations in the original 12 single point mutants were located far from the active site (Figure 3a). Indeed, all of the T_m data support the model of intramolecular interactions driving mutant stability suggested by the analysis in Supporting Information: Figure S2.

10970290, 0, Downloaded from https://onlinelibrary.wiley.com/doi/10.1002/bit.28319 by Cornell University, Wiley Online Library on [26/01/2023]. See the Terms and Conditions (https://onlinelibrary.wiley.com/terms-and-conditions) on Wiley Online Library for rules of use; OA articles are governed by the applicable Certavier Commons License

Semi-rational PETase mutants and source algorithms TABLE 1

R AND GODDA	.RD																	BIC	TEC	CHN	OLC)GY	-W	'IL	ΕY	
Chosen mutation (s)			A475,A47R		_,	,				T72S, T72V			۵	J.	S	V134T, V134L	Ω	DIC Z	ENC		EEKI	O		N173F, N173R		
	N37A	S46T	A47S	T51A	R53Q	S54W	S58L	R59S	1897	T72S,	N73S	A74P	S124A	M128L	R132S	V134	S136D	G139N	T140F	S142D	Y146H	K148Q	79A	N173	A180M	Q182L
PROSS recommended mutation	None	None	None	None	None	None	None	None	None	None	None	None	⋖	None	None	None	None	z	œ	None	None	None	4	œ	Σ	None
FireProt recommended mutation	None	None	œ	⋖	None	*	None	S	_	None	S	None	None	_	None		None	None	None	None	~	~	٨	ш	None	_
Rosetta beneficial mutations (most to neutral)	Y,A,E,W,F,H,M,T,R	К,T	S,L,M,F,V,T,Y,H,K	F,A,Q,E,L,M,S,Y,I,R,G,P,N,V	Q,K,S,A,F,H	F,W,Y,K,H,R,T,E,D,L,M,C,N,A	L,Q,V,E,K,A,N,T,C,R,D,Y,I	S,N	W,D	K,Q,V,S,R,I,A	H,Y,L,E,S	۵	А	>	W,M,S,K,V,A,G,T,Y,H,F,L,N,I,Q,E,D	-	K,F,M,R,T,V,D,I,N,E,W,Y,L,Q,H,G	N,K,F,T,I,Q,V,Y,C,S,A,L,R,E,D,H,M	ш	Γ,D	I	W,Q,N,M,F,L,R,H,A,I,Y,T,E,S,G	None	Y,F,W,H,Q,I,R,L,K,V,A,M	None	None
HotSpot wizard positive/neutral mutations (most to least likely to preserve function)	A,D,F,L,M,S,C,Q,V,H,E,G,T,R,K,P	A,C,F,D,H,Q,M,V,L,T,N,G,R,E,K,P,Y,I	D,K,Q,R,S,H,L,M,T,Y,F,E,C,V,N,G,Y,I	A,D,Q,S,F,H,L,M,V,E,R,C,N,K,G,Y,I,P	D,Q,S,A,H,F,L,M,K,E,T,V,C,N,Y,G,I,W	H,T,Q,D,K,F,R,C,M,V,L,Y,A,E,N,G,W	A,G,L,C,F,H,T,M,V,D,Q,N,E,P,R,K,I,Y	Q,V,D,F,M,S,C,H,L,A,N,T,E,K,G,Y,I,P,W	I,F,L,M,V	S,H,C,F,D,V,L,M,Q,A,N,R,G,K,E,I,Y	D,S,C,H,V,F,T,M,A,L,Q,G,E,I,R	S,T,C,F,H,D,L,V,M,Q,N,G,E,R,I,K,P	A,G,C,F,V,H,M,D,E,N,Q,T,L,P,R,K,I,Y	L,Q,A,F,V,D,E,K,R,S,H,I,N,T,C,Y,W	S,D,Q,H,N,F,K,M,V,E,T,AC,L,Y,G,I,W	L,M,F,A,C,S,T,Q	Q,D,A,H,C,F,V,M,L,N,T,E,G,R,K,I,P,Y	N,D,H,Q,S,T,A,C,V,E,K,F,R,M,L,I,Y,P,W	K,D,Q,R,S,H,M,L,F,Y,A,V,E,C,N,W,G,I	H,C,D,T,A,F,G,M,V,Q,L,N,E,P,R,K,I,Y	K,G,R,D,S,L,M,H,A,E,F,V,T,C,N,W,1,G	Q,R,L,M,E,A,D,W,F,I,S,V	A,L,F,M,V,Q,C,E,D	D,Q,R,K,S,H,L,M,A,E,F,Y,V,T,C,W,I,G	I,V,F,L,M,S,C,H,T,N,Q,D	L,M,F,A,V,S,C,H,T,D,E,K,N,R,I,Y
HotSpot wizard relative flexibility	High	High	Moderate	High	High	High	High	High	Moderate	High	High	Moderate	Low	Low	Moderate	Moderate	High	High	High	High	High	High	Low	Low	Low	Low
HotSpot wizard mutability	High	High	High	High	High	High	High	High	Moderate	High	High	High	High	High	High	Moderate	High	High	High	High	High	Moderate	Moderate	High	Moderate	Moderate
WT identity	z	S	∢	⊢	ď	S	S	œ	>	⊢	z	∢	S	Σ	œ	>	S	U	-	S	>	¥	S	z	∢	σ
Residue	37	46	47	51	53	54	28	59	89	72	73	74	124	128	132	134	136	139	140	142	146	148	169	173	180	182

10970290, 0, Downloaded from https://onlinelibrary.wiley.com/doi/10.1002/bit.28319 by Cornell University, Wiley Online Library on [26/01/2023]. See the Terms and Conditions (https://onlinelibrary.wiley.com/terms-and-conditions) on Wiley Online Library for rules of use; OA articles are governed by the applicable Cerative Commons License

_
ס
Ð
\exists
_
.=
+
$\overline{}$
$\overline{}$
O
()
ະ
-
E 1
ш
Щ

Residue	WT	HotSpot wizard mutability	HotSpot wizard relative flexibility	HotSpot wizard positive/neutral mutations (most to least likely to preserve function)	Rosetta beneficial mutations (most to neutral)	FireProt recommended mutation	PROSS recommended mutation	Chosen mutation (s)
186	۵	High	High	H,N,S,C,T,V,F,Q,K,M,Y,L,A,E,I,R,G,W	S,A,H,N,Y	z	None	D186H, D186N
187	S	High	High	D,C,F,L,T,V,G,M,A,H,N,Q,P,E,R,I,K	N,L,Y,T,D,I,W,F,A,M,Q,K	None	T,P	S187T
188	S	High	High	N,D,H,C,T,V,F,Q,M,A,K,L,R,Y,E,G,I,W,P	H,Q,L,F,A,Y,T,N,M,K	None	None	S188H
190	z	High	High	M,D,H,K,Q,S,T,C,Y,A,F,R,V,E,L,G,Q,I,P	F,Y,S,Q,W,A,D,V,K	None	None	N1190Q
193	S	High	High	C,N,Q,D,H,V,T,A,M,E,F,K,R,G,L,Y,I,P,W	M,R,Y	None	None	S193R
205	z	High	High	C,D,S,F,H,V,M,Q,L,T,A,E,K,R,Y,G,I,W	F,W	None	None	N205F
207	S	High	High	L,M,V,C,D,F,H,Q,T,A,K,R,N,E,G,Y,P,I,W	None	None	None	S207T
210	۵	High	High	S,C,G,T,D,F,H,M,V,A,L,N,Q,E,R	Q,V,H,E	None	None	P210H
212	z	High	High	M,Q,A,D,S,F,H,L,C,V,E,R,T,K,G,Y,I,P,W	Y,E,S,C,H,W,F,L	None	None	N212S
214	S	Moderate	Moderate	H,T,Y,D,F,C,V,K,N,Q,M,L,R	F,Y,H,Q,T,E,K,R	I	Υ,Н	S214Y, S214H
222	Σ	Moderate	Moderate	L,F,I,V,A,S,T,C,Q,H,N,E,D	None	٦	None	M222L
223	S	Moderate	Moderate	P,T,G,H,D,C,A,Q,V,F,L,M,K,N,R,E,Y	H,Y,I,V,F,K	۵	None	S223Н
224	œ	High	High	H,S,T,D,C,A,F,Q,V,M,L,N,G,E,K,I,P,Y	W,Q,F,N,V,Y,S,T,L	None	None	R224Q
232	_	Moderate	Moderate	M,L,F,V,S,A,C,H,T,D,N,Q	>	7	None	1232V
233	z	High	High	R,A,D,S,E,H,Q,K,F,M,T,V,C,L,Y,G,I,W,P	M,R	None	None	N233R
238	S	High	Moderate	M,F,L,C,D,H,Q,N,T,A,E,K,R,Y,G,I,W	*	ш	None	S238F
245	S	High	High	G,C,D,H,F,V,A,M,T,L,N,Q,E,P,R,K,I,Y	Y,T,L,E,A,N,W,Q,P,F,K,M,R	z	None	S245N
247	σ	High	Moderate	D,N,S,H,C,T,V,F,M,A,E,K,Y,I,L,R,G,W	R,L,W,Y,V,K,S,I,T,N,F,M,E,A	None	None	Q247N
248	_	High	Moderate	D,Q,C,F,H,S,T,V,M,A,N,G,E,K,R,Y,I,P	S,Y,K,R,Q,F,T,M	None	D	L248S
250	_	High	Moderate	F,M,V,L,S,A,T,C,H,Q,D,N,E,R,K	٦	None	None	1250L
266	⊢	High	High	H,S,D,C,F,Q,V,L,M,A,N,G,R,E,K,I,Y,P	S,L,I,V,Q,R,N	None	None	T266S
274	ш	High	Moderate	P,S,D,G,C,H,Q,T,V,A,M,K,L,N,R,F,Y	L,S,I,W,G,T,V,N,A	None	None	E274G
280	œ	High	High	A,D,L,M,Q,F,S,V,H,E,K,C,T,N,Y,G,I,W	W,L,D,S	None	None	R280L
283	۵	High	High	E,Q,A,R,K,M,L,S,F,V,H,N,Y,C,T,W,I	M,N,L,R,E,A,S,T,Q	None	None	D283E
288	z	Moderate	High	H,D,S,Q,T,C,F,V,M,A,E,K,L,R,I,G,Y	K,Y,F,R,H,Q,E,W,L	ш	None	N288R
290	S	Moderate	High	H,D,C,G,Q,A,P,T,M,K,V,E,N,R,L	Y,G,K,W,E,P,A,N,L	~	None	S290E

-conditions) on Wiley Online Library for rules of use; OA articles are governed by the applicable Creative Commons License

A S	46T	A47S	A47R	T51A	R53Q	S54W	S58L
s v	681	T72S	T72V	N73S	A74P	S124A	M128L
2S Q1	33Y \	V134L	V134T	S136D	G139N	T140F	S142D
6H K1	48Q 3	S169A	N173F	N173R	A180M	Q182L	D186H
6N S1	87T S	S188H	N190Q	S193R	N205F	S207T	P210H
2S S2	14H	S214Y	M222L	S223H	R224Q	1232V	N233R
8F N2	418	S245N	Q247N	A248S	1250L	WT	T270Q
4G T2	79L I	R280L	D283E	N288R	S290E	Dead	Blank
							7215
-	9S V 32S Q1 6H K1 6N S1 2S S2 8F N2	98 V68I 22S Q133Y 6H K148Q 6N S187T 2S S214H 8F N241S 4G T279L	98 V68I T728 428 Q133Y V134L 66H K148Q S169A 66N S187T S188H 28 S214H S214Y 48F N241S S245N 4G T279L R280L	9S V68I T72S T72V 12S Q133Y V134L V134T 6H K148Q S169A N173F 16N S187T S188H N190Q 12S S214H S214Y M222L 18F N241S S245N Q247N 4G T279L R280L D283E	9S V68I T72S T72V N73S 12S Q133Y V134L V134T S136D 6H K148Q S169A N173F N173R 16N S187T S188H N190Q S193R 2S S214H S214Y M222L S223H 18F N241S S245N Q247N A248S 4G T279L R280L D283E N288R	98 V68I T72S T72V N73S A74P 128 Q133Y V134L V134T S136D G139N 16H K148Q S169A N173F N173R A180M 16N S187T S188H N190Q S193R N205F 128 S214H S214Y M222L S223H R224Q 18F N241S S245N Q247N A248S 1250L 14G T279L R280L D283E N288R S290E	98 V68I T72S T72V N73S A74P S124A 12S Q133Y V134L V134T S136D G139N T140F 6H K148Q S169A N173F N173R A180M Q182L 16N S187T S188H N190Q S193R N205F S207T 12S S214H S214Y M222L S223H R224Q I232V 18F N241S S245N Q247N A248S I250L WT 14G T279L R280L D283E N288R S290E Dead

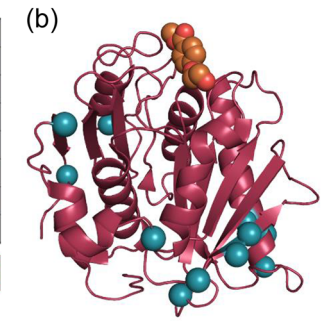


FIGURE 3 High-throughput activity screens reveal a subset of highly active PETase point mutants. (a) Heat map of depolymerase activity as measured by fluorescence (ex. 328 nm, em. 421 nm). Colors represent average of three technical replicates. Activity is shown on a scale of white (low) to teal (high). "Dead" refers to negative control active site mutant (S160A/D206A/H237A) with no possible depolymerase activity; "Blank" refers to negative control containing no expressed protein. Mutants with significantly higher activity than wild-type across two separate biological replicates are highlighted with heavy outlines and bold font. Color bar below heat map indicates range of RFU depicted in map. (b) Location of highly active mutants on PETase structure. Mutants with significantly higher activity than wild-type are highlighted with teal spheres at their alpha carbons. MHET is shown in orange spheres to give perspective on the location of the active site.

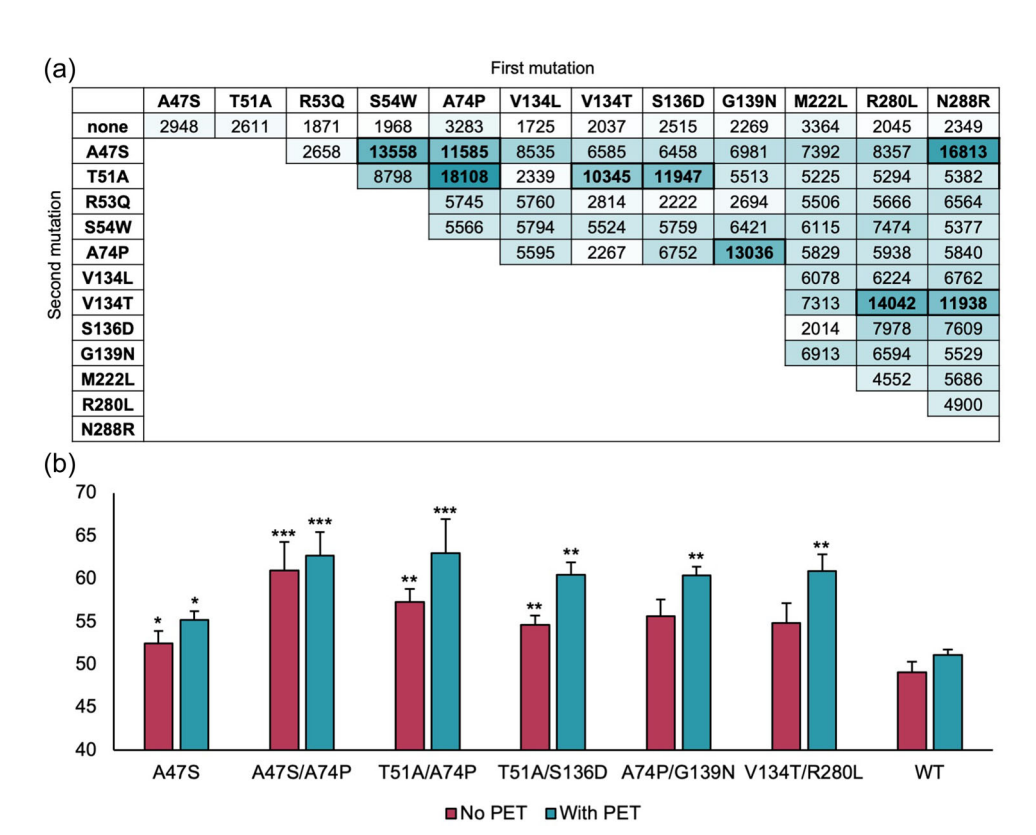


FIGURE 4 Combining high-performing mutations produces synergistic effects. (a) Depolymerase activity of single and double mutants as measured by fluorescence (ex. 328 nm, em. 421 nm). Colors represent average of three technical replicates. Activity is shown on a scale of white (low) to teal (high). Double mutants with synergy, defined as significantly higher activity than both of their parent mutants, are highlighted with heavy outlines and bold font. (b) Apparent melting points of wild-type PETase and mutants with significant increases in stability. Error bars indicate standard deviation of three biological replicates. Stars above rose-colored bars indicate significantly higher T_m than WT PETase in the presence of PET. Significance was determined by unpaired two-tailed T test, with *0.01 < p < 0.05, **0.001 < p < 0.01, and ***p < 0.001.

3.5 | Role of oligomeric PET in quantifying degradation activity

Because the high-throughput PETase engineering platform utilizes fluorescence spectroscopy to detect depolymerase activity, the data

must be processed differently than the outputs of experiments conducted with liquid chromatography. We constructed standard curves of oxidized bis- (2-hydroxyethyl) terephthalate (BHET-OH), mono- (2-hydroxyethyl) terephthalate (MHET-OH), and terephthalic acid (TPA-OH), the three degradation products analyzed by previous

10970290, 0, Downloaded from https://onlinelibrary.wiley.com/doi/10.1002/bit.28319 by Cornell University, Wiley Online Library on [26/01/2023]. See the Terms and Conditions (https://onlinelibrary.wiley.com/

on Wiley Online Library for rules of use; OA articles are governed by the applicable Creative Commons License

PETase studies (Supporting Information: Figure S4). TPA-OH had the strongest fluorescent signal, followed by MHET-OH and BHET-OH, respectively (Supporting Information: Figure S4). This is consistent with previously reported data (Ebersbach et al., 2012) and shows that fluorescent product detection is possible for all three major PET monomers. MHET is the major product of PETase catalysis (Yoshida et al., 2016), while both TPA and BHET are consistently observed as minor products (Cui et al., 2021; Lu et al., 2022; Son et al., 2019). There is some evidence that different expression systems such as Yarrowia lipolytica may convert PET directly into TPA and ethylene glycol (Kosiorowska et al., 2022). While MHET-OH has a lower fluorescent extinction coefficient than TPA-OH, because all three oxidized monomeric degradation products are fluorescent, signal will increase proportionately with degradation product concentration, though it is not possible using this method to quantify which fraction of the products corresponds to each monomer species.

While we were able to observe linear correlations between fluorescence and concentration in all three standard curves, the outputs were not of a magnitude consistent with the outputs of the enzymatic assays (thus, data are presented in a log₁₀ scale while correlations follow linear regression in Supporting Information: Figure S4). Rather, PETase degradation products had net fluorescence corresponding to product concentration higher than theoretically possible given constraints of product solubility and substrate concentration. The fluorescence of oxidized monomers was therefore found to not be adequate in explaining PETase activity, likely because monomers are not the only output of PETase activity

(Pirillo et al., 2021). Indeed, PETase also produces oligo (ethylene terephthalate) (OET) (Schubert et al., 2022) defined here as any soluble PET hydrolysis product containing more than one terephthalate unit. Because OET has, by definition, multiple aromatic groups, its oxidation products will in turn have higher extinction coefficients than its monomeric counterparts, increasing fluorescent signal. This insight highlights a fundamental limitation of PETase activity studies that rely on chromatographic methods to detect degradation products. Because OET products are inherently heterogeneous, and because standards must be used to define target analytes, chromatographic techniques do not account for OET in PETase activity studies. However, for purposes of biodegradation, OET is as desirable a byproduct as monomeric BHET, MHET, or TPA due to its solubility, which enables it to interface with the microbial world and, eventually, be assimilated. Therefore, ability to detect both monomeric and oligomeric products of PET biodegradation is an important benefit of spectroscopic detection, though it does change how the data are analyzed.

3.6 | Defining new metrics for quantifying PETase activity

To develop a method to effectively compare PETase mutants using fluorescence spectroscopy, we defined a new series of metrics (Figure 5). Because fluorescent signal corresponds to multiple degradation products, we chose to leave the outputs of the PETase

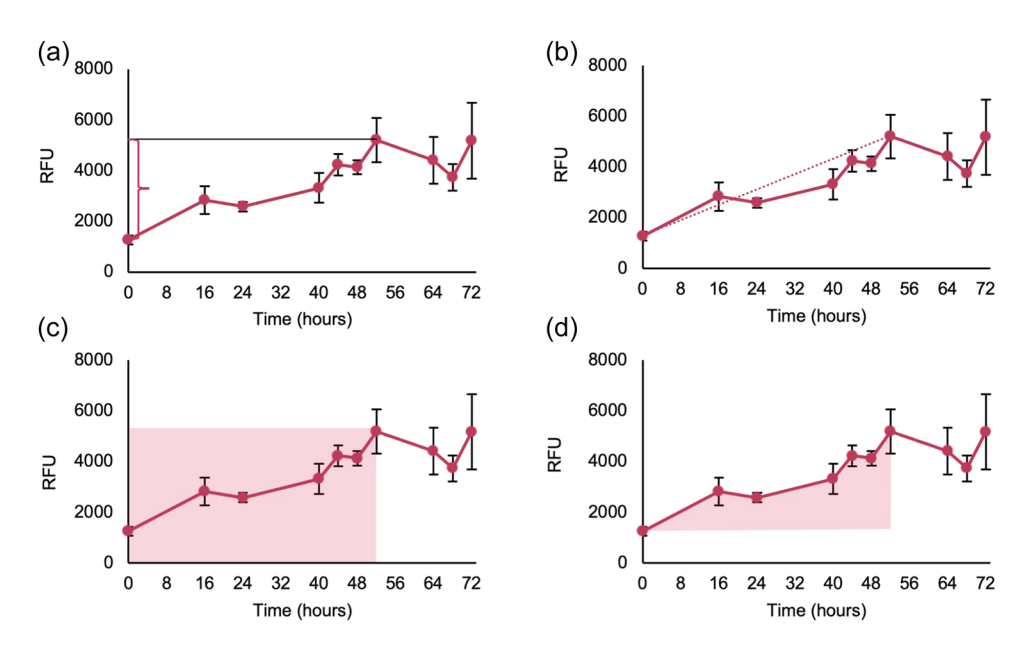


FIGURE 5 Definition of relevant parameters for fluorescent quantification of PETase activity, showing wild-type PETase activity measured by fluorescence (ex. 328 nm, em. 421 nm). Points indicate average fluorescence of three technical replicates. Error bars are standard deviation. (a) Maximum product concentration is defined as the difference between baseline fluorescence and maximum fluorescence. (b) Depolymerase velocity is defined as the slope of the line fitted to the timepoints between time t = 0 and the time at which the maximum fluorescence occurs. Lines were fitted using linear regression in GraphPad Prism 7. (c) Activity duration is defined as the time in hours at which the maximum product fluorescence occurs. (d) Total product released × activity duration is defined as the area under the kinetic curve from time t = 0 to the time at which the maximum product fluorescence occurs. Area under the curve was determined using GraphPad Prism 7.

degradation as relative fluorescence units, which comprises all aromatic hydrolytic products in undetermined proportions. Thus, maximum fluorescence does not necessarily correspond to maximum degradation. Indeed, we observed fluorescence decreasing somewhat over time in some samples, which we attribute to OET hydrolysis releasing monomers, increasing degradation product concentration while decreasing fluorescence because the monomers have lower extinction coefficients than OET. However, because peak fluorescence was straightforward and unambiguous to identify, we chose to compare PET mutants by their maximum product fluorescence to ensure uniformity of measurement (Figure 5a). Maximum product fluorescence (Figure 5a) is a proxy for concentration of degradation products, but more information can be gleaned from kinetic data, including average velocity (Figure 5b), activity duration (Figure 5c), and total product released × activity duration (Figure 5d). Together, this quartet of metrics comprehensively describe enzymatic activity and stability, as well as a holistic combination of the two.

Total product released × activity duration is a particularly useful metric because it contains both kinetic and thermodynamic parameters but has some bias toward thermostability. If two mutants reach

the same level of degradation, but one takes twice as long to get there, that enzyme will have twice the total product released× activity duration score because it was active for twice as long. Longer activity duration is important when considering biodegradation of microplastic mixtures with heterogeneous crystallinity because substrate crystallinity has a significant impact on PETase degradation kinetics (Pasula et al., 2022). We thus screened mutants on a single lot of PET fibers, presumably uniform in crystallinity and any gains in reaction velocity may not translate to substrates of differing crystallinity. Therefore, increased activity duration, which is a property of the enzyme itself and independent of substrate crystallinity, is a more important parameter to screen for than depolymerase velocity, though the latter is still useful. Combining the two metrics with a bias toward activity duration in total product released × activity duration gives a single value that can be compared across mutants in kinetic PETase analyses.

We used these metrics to compare activity between the synergistic double mutants, their corresponding parent single mutants, and wild-type PETase (Figure 6, Supporting Information: Figure S5). We found that maximum product fluorescence was significantly higher in some mutants than in wild-type PETase (Figure 6a, Supporting Information: Figure S5A),

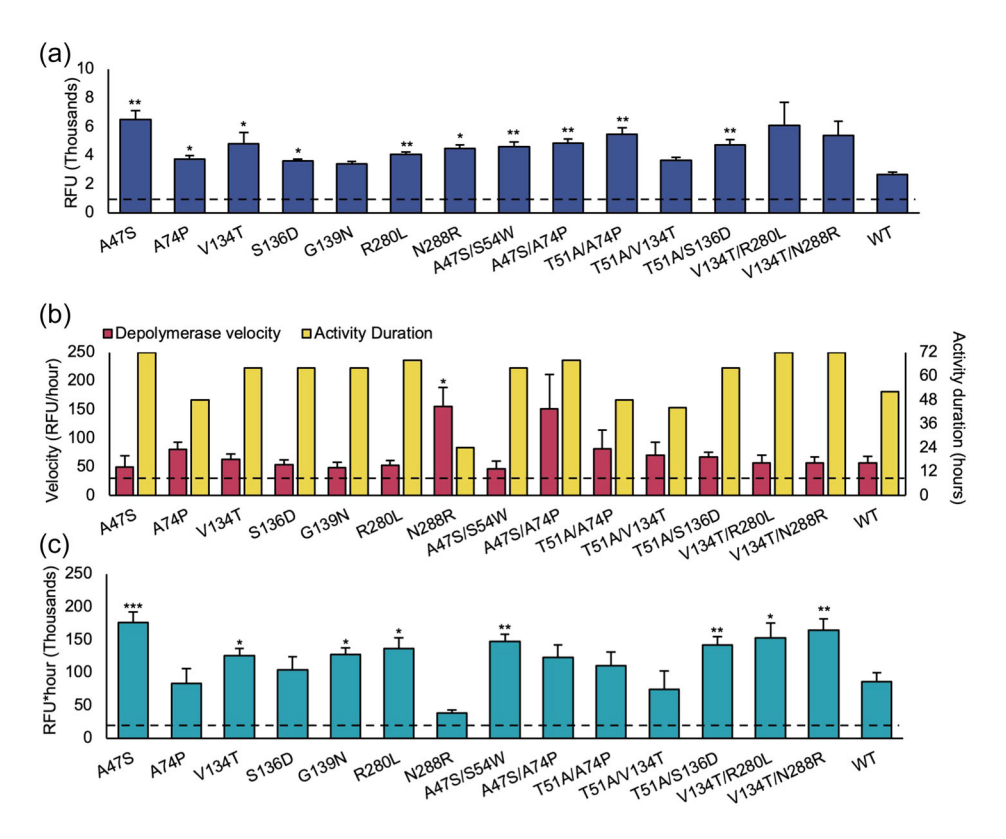
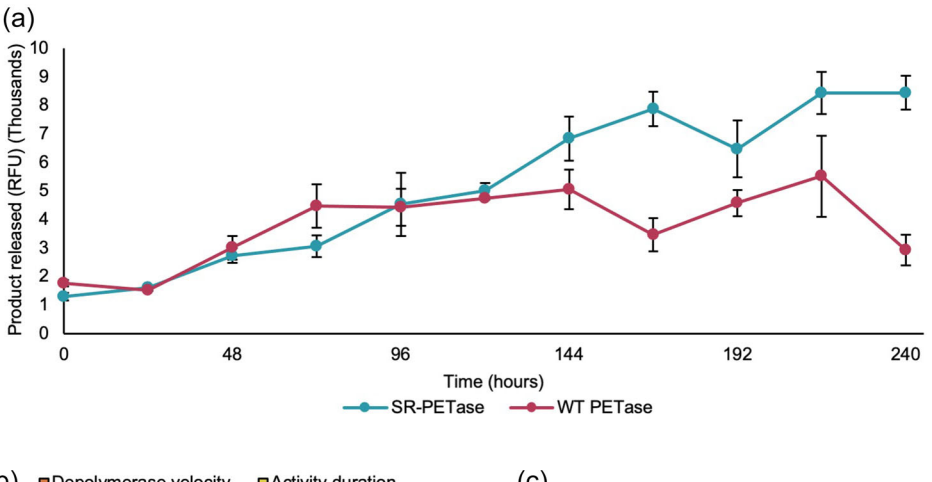


FIGURE 6 Point mutant subset shows significant increases in activity and stability metrics over wild-type PETase. All data are shown as average of three technical replicates. Data are representative of three separate biological replicates. Significance was determined by comparison to wild-type values by unpaired two-tailed T test, with *0.01 < p < 0.05, ** 0.001 < p < 0.01, and *** p < 0.001. Error bars indicate standard error of the mean. Dashed lines indicate activity values of negative control active site mutant (\$160A/D206A/H237A). Only mutants with significant differences from the wild-type enzyme are shown. The complete set of mutants analyzed is displayed in Supporting Information: Figure S5. (a) Maximum fluorescence of PET degradation products during 72-hour time course. (b) Depolymerase velocity and activity duration of mutants. Velocity is plotted as rose-colored bars on the left axis, duration is plotted as yellow bars on the right axis. (c) Total product released × activity duration of mutants.



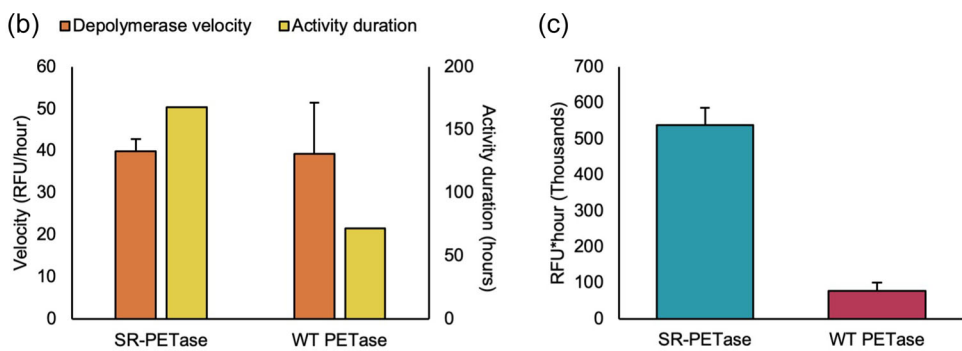


FIGURE 7 SR-PETase outperforms WTPETase across the range of activity and stability metrics. (a) Comparison of WT- and SR-PETase across a 240 h time course. Values represent means of n = 3 determinations with error bars indicating standard deviation. (b) Depolymerase velocity and activity duration of mutants. Velocity is plotted as orange bars on the left axis, duration is plotted as yellow bars on the right axis. Error bars indicate standard error of the mean. (c) Total product released × activity duration of WT PETase and SR-PETase. Error bars indicates standard error of the mean.

even as velocity was not significantly affected by the mutations (Figure 6b). Rather, the driving force in increasing product fluorescence was the increased duration of activity in PETase mutants relative to the wild-type enzyme (Figure 6b, Supporting Information: Figure S5B). Increased activity duration correlated strongly with increased $T_{\rm m}$ (Figures 4b and 6b, Supporting Information: Figures S3 and S5B), The holistic total product released × activity duration metric was able to reconcile the discrepancies between velocity and maximum fluorescence (Figure 6c, Supporting Information: Figure S5C), highlighting its utility as a general method of comparing PETase mutants.

3.7 | Combinatorial mutagenesis yields a highly active PETase variant

After observing the synergistic effects of combining point mutations, we used a combinatorial approach to optimize PETase activity within the parameters of this study. We subjected these multimutants (variants with >2 residues mutated from wild-type PETase) to a 10-day kinetic study, with product release analysis every 24 h. As previously observed, wild-type PETase lost all activity after 72 h, while the most successful multimutant, A47S/T51A/A74P/V134T/G139N/R280L/N288R, which we refer to as SR-PETase due to the semi-rational mutagenesis design,

continued releasing PET degradation products for up to 168 h (Figure 7a,b for SR-PETase kinetic profile; full data set for all multimutants available in Supporting Information: Figure S6). When analyzed according to the metrics defined in Figure 5, SR-PETase has about 1.9-fold higher maximum product fluorescence and about 7.4-fold higher total product released × activity duration than wild-type PETase over 10 days at 40°C (Figure 7a,c). Interestingly, there is no significant difference in reaction velocity between the two enzymes (Figure 7b), indicating that the increase in activity is driven solely by increased stability, which again is consistent with the hypothesized roles of the mutations detailed in Supporting Information: Figure S2. The development of SR-PETase through use of high throughput screening of a semi-rational mutant library shows that the PETase engineering platform presented in this study can successfully produce highly stable enzyme variants with only three rounds of iterative mutagenesis.

4 | CONCLUSIONS

In this study, we developed a high-throughput PETase expression and screening platform and validated its utility by creating a PETase variant with between 1.9 and 7.4-fold higher activity (depending on the metric used) than the wild-type enzyme over 10 days at 40° C. By

and-conditions) on Wiley Online Library for rules of use; OA

articles are governed by the applicable Creative Commons License

from https://onlinelibrary.wiley.com/doi/10.1002/bit.28319 by Cornell University, Wiley Online Library on [26/01/2023]. See the Terms and Conditions (https://onlinelibrary.wiley.com/terms.com/doi/10.1002/bit.28319 by Cornell University, Wiley Online Library on [26/01/2023]. See the Terms and Conditions (https://onlinelibrary.wiley.com/terms.com/doi/10.1002/bit.28319 by Cornell University, Wiley Online Library on [26/01/2023]. See the Terms and Conditions (https://onlinelibrary.wiley.com/terms.com/term

integrating secretory protein expression with fluorescent product detection, this platform streamlines PETase mutant evaluation, enabling near-simultaneous screening of 96 samples. The high throughput of this platform enabled us to build on previous PETase research through evaluation of a larger mutant library than the rational and computational approaches previously employed. Direct characterization of the PET degradation of expression supernatant without enzyme concentration normalization further streamlined screening and supported our applications driven goal of increasing PET degradation. Nevertheless, future work in which expression kinetics and enzyme concentration are characterized for a subset of optimally performing mutants will permit formal kinetic analysis. We pursued a semi-rational protein engineering approach, screening 57 point mutations, 54 of which are new to this study. Of these mutants, 12 were found to have significantly higher activity than wild-type PETase across multiple biological replicates. Diving deeper into the biochemistry of the mutant residues, we found that the observed increases in activity could all be explained by enhanced stability of the mutated protein (Supporting Information: Figure S2). To validate this model, we performed differential scanning fluorimetry, which revealed that the mutated enzymes did indeed have enhanced thermostability relative to their wild-type counterpart. The stabilization hypothesis was further corroborated through analysis of time course data using a series of metrics developed to decouple the effects of increased reaction velocity and increased catalytic stability. We found that, though successful PETase mutants did not have significantly higher velocity than wild-type PETase, they did remain active for a longer duration and that this enhanced stability resulted in significantly higher amounts of degradation products. While the fluorescence detection of PET degradation products performed here facilitated a higher throughput characterization of mutants, chromatographic characterization of degradation products will be a necessary future direction to more thoroughly quantify degradation products. When successful mutants were combined to yield SR-PETase (with 7-point mutations), the stability was further increased. with the maximum degradation product concentration being reached after 168 h of incubation, even as wild-type PETase lost activity within 72 h. Future experiments conducted at higher temperatures closer to the glass transition temperature of PET would be interesting to explore observations of previous reports in which mutants with melting temperatures nearing the glass transition temperature of the microplastic target substrate experience enhanced performance (Lu et al., 2022). Additional analysis of degradation kinetics of different commercial forms of PET (e.g., film, powder, varying levels of crystallinity) would also provide greater clarity on which mutations will be advantageous in industrially relevant settings.

Comparison of SR-PETase to published mutants was not directly possible due to the difference in expression system (protein concentration was not normalized between wells in this study), detection methodology, and model substrate. However, qualitative analysis of activity relative to wild-type PETase shows that SR-PETase has a similar magnitude of improvement as compared to other published mutants. For example, TS-PETase is reported to have between 5 and 7 fold higher

activity than wild-type PETase (Zhong-Johnson et al., 2021), Thermo-PETase has up to 14-fold improved activity (Son et al., 2019), and FAST-PETase has up to 29-fold improved activity (Lu et al., 2022). The 1.9-7.4-fold improvement observed in SR-PETase is therefore comparable to the state of the art and demonstrates the utility of the highthroughput platform for PETase engineering.

The results presented in this work make progress toward industrial application of PETase for larger scale microplastic degradation. We have engineered PETase to retain hydrolytic activity for significantly longer than wild-type PETase at industrially relevant temperatures. More broadly, we have built a framework for highthroughput PETase engineering that tolerates a variety of reaction conditions. To enable quantification of PETase activity using this engineering platform, we have developed a series of metrics: maximum product concentration, depolymerase velocity, activity duration, and total product released × activity duration. These metrics enable direct comparison of mutants screened by the platform presented and decouple kinetic and thermodynamic effects on overall activity, enabling a deeper understanding of the catalysts produced by the engineering process. Adaptation of the reported screening method to alternate plastic degrading enzymes using secretory expression and alternative fluorescent or colorimetric degradation product quantification remains an interesting opportunity for future research. Overall, we have advanced the state of the field by increasing the potential throughput and chemical flexibility of future PETase engineering studies, enabling facile re-optimization of enzymatic activity in conditions pertinent to the desired end-use application.

AUTHOR CONTRIBUTIONS

Hannah S. Zurier conceived of the study, performed all experiments, wrote the original manuscript draft and supported funding acquisition. Julie M. Goddard supervised the research, provided resources and project administration, and acquired funding. Both authors designed experiments, analyzed data and reviewed and edited the manuscript.

ACKNOWLEDGMENTS

This work was supported by the United States Department of Agriculture by the National Institute of Food and Agriculture Award No. 2021-67019-33686 and Hatch Accession No. 1023604). Sanger DNA sequencing was performed by the Cornell Biotechnology Resource Center (RRID:SCR_021727). Differential scanning calorimetry was performed at the Cornell Center for Materials Research, which is supported by the National Science Foundation under Award Number DMR-1719875. The authors thank Dr. Martin Wiedmann for allowing access to the QuantStudio Real-Time PCR system in his lab. The DNA sequence of YebF was provided by the laboratory of Dr. Matthew P. DeLisa at Cornell University. DSF data was collected by Ian Kay and Halle Redfearn.

CONFLICT OF INTEREST

The authors declare no conflict of interest.

DATA AVAILABILITY STATEMENT

The data that supports the findings of this study are available in the supplementary material of this article.

ORCID

Hannah S. Zurier http://orcid.org/0000-0002-6576-148X Julie M. Goddard http://orcid.org/0000-0002-3644-0732

REFERENCES

- Ariza-Tarazona, M. C., Villarreal-Chiu, J. F., Hernández-López, J. M., Rivera De la Rosa, J., Barbieri, V., Siligardi, C., & Cedillo-González, E. I. (2020). Microplastic pollution reduction by a carbon and nitrogendoped TiO2: Effect of pH and temperature in the photocatalytic degradation process. *Journal of Hazardous Materials*, 395, 122632.
- Austin, H. P., Allen, M. D., Donohoe, B. S., Rorrer, N. A., Kearns, F. L., Silveira, R. L., Pollard, B. C., Dominick, G., Duman, R., El Omari, K., Mykhaylyk, V., Wagner, A., Michener, W. E., Amore, A., Skaf, M. S., Crowley, M. F., Thorne, A. W., Johnson, C. W., Woodcock, H. L., ... Beckham, G. T. (2018). Characterization and engineering of a plastic-degrading aromatic polyesterase. *Proceedings of the National Academy of Sciences*, 115, E4350–E4357. https://www.pnas.org/content/115/19/E4350
- Bååth, J. A., Borch, K., Jensen, K., Brask, J., & Westh, P. (2021). Comparative biochemistry of four polyester (PET) hydrolases. ChemBioChem, 22, 1627–1637.
- Chen, C. C., Han, X., Ko, T. P., Liu, W., & Guo, R. T. (2018). Structural studies reveal the molecular mechanism of PETase. *The FEBS Journal*, 285, 3717–3723. https://onlinelibrary.wiley.com/doi/full/10.1111/febs.14612
- Cui, Y., Chen, Y., Liu, X., Dong, S., Tian, Y., Qiao, Y., Mitra, R., Han, J., Li, C., Han, X., Liu, W., Chen, Q., Wei, W., Wang, X., Du, W., Tang, S., Xiang, H., Liu, H., Liang, Y., ... Wu, B. (2021). Computational redesign of a PETase for plastic biodegradation under ambient condition by the GRAPE strategy. ACS Catalysis, 11, 1340–1350. https://pubs.acs.org/doi/abs/10.1021/acscatal.0c05126
- Ebersbach, H., Geisse, S., Vincent, K. J., Zurini, M., Mcneely, P. M., Naranjo, A. N., Robinson, A. S., Lingg, N., Zhang, P., Song, Z., Bardor, M., Van Beers, M. M. C., Kallberg, K., Johansson, H.-O., Bulow, L., Godawat, R., Brower, K., Jain, S., Konstantinov, K., ... Mandenius, C.-F. (2012). A high-throughput assay for enzymatic polyester hydrolysis activity by fluorimetric detection. *Biotechnol Journal*, 7, 1517–1521. https://onlinelibrary.wiley.com/doi/full/10.1002/biot.201200119
- Fecker, T., Galaz-Davison, P., Engelberger, F., Narui, Y., Sotomayor, M., Parra, L. P., & Ramírez-Sarmiento, C. A. (2018). Active site flexibility as a hallmark for efficient PET degradation by I. sakaiensis PETase. Biophysical Journal, 114, 1302–1312.
- Geyer, R., Jambeck, J. R., & Law, K. L. (2017). Production, use, and fate of all plastics ever made. *Science Advances*, 3, e1700782.
- Godoy, V., Blázquez, G., Calero, M., Quesada, L., & Martín-Lara, M. A. (2019). The potential of microplastics as carriers of metals. *Environmental Pollution*, 255, 113363.
- Goldenzweig, A., Goldsmith, M., Hill, S. E., Gertman, O., Laurino, P., Ashani, Y., Dym, O., Unger, T., Albeck, S., Prilusky, J., Lieberman, R. L., Aharoni, A., Silman, I., Sussman, J. L., Tawfik, D. S., & Fleishman, S. J. (2016). Automated structure- and sequence-based design of proteins for high bacterial expression and stability. *Molecular Cell*, 63, 337–346.
- Gong, J., Kong, T., Li, Y., Li, Q., Li, Z., & Zhang, J. (2018). Biodegradation of microplastic derived from poly(ethylene terephthalate) with bacterial whole-cell biocatalysts. *Polymers*, 10, 1326. https://www.mdpi.com/ 2073-4360/10/12/1326/htm

- Hadad, D., Geresh, S., & Sivan, A. (2005). Biodegradation of polyethylene by the thermophilic bacterium Brevibacillus borstelensis. *Journal of Applied Microbiology*, 98, 1093–1100. https://onlinelibrary.wiley.com/doi/full/10.1111/j.1365-2672.2005.02553.x
- Ho, B. T., Roberts, T. K., & Lucas, S. (2017). An overview on biodegradation of polystyrene and modified polystyrene: The microbial approach. *Critical Reviews in Biotechnology*, 38, 308–320. https://www.tandfonline.com/doi/abs/10.1080/07388551.2017. 1355293
- Huang, X., Cao, L., Qin, Z., Li, S., Kong, W., & Liu, Y. (2018). Tatindependent secretion of polyethylene terephthalate hydrolase PETase in bacillus subtilis 168 mediated by its native signal peptide. *Journal of Agricultural and Food Chemistry*, 66, 13217–13227. https://doi.org/10.1021/acs.jafc.8b05038. https://pubs.acs.org/doi/full/
- Huynh, K., & Partch, C. L. (2015). Analysis of protein stability and ligand interactions by thermal shift assay. *Current Protocols in Protein Science*, 79, 28.9.1–28.9.14.
- Joo, S., Cho, I. J., Seo, H., Son, H. F., Sagong, H. Y., Shin, T. J., Choi, S. Y., Lee, S. Y., & Kim, K. J. (2018). Structural insight into molecular mechanism of poly(ethylene terephthalate) degradation. *Nature Communications*, 9, 382. https://www.nature.com/articles/s41467-018-02881-1
- Koshti, R., Mehta, L., & Samarth, N. (2018). Biological recycling of polyethylene terephthalate: A mini-review. *Journal of Polymers and the Environment*, 26, 3520–3529. https://link.springer.com/article/ 10.1007/s10924-018-1214-7
- Kosiorowska, K. E., Moreno, A. D., Iglesias, R., Leluk, K., & Mirończuk, A. M. (2022). Production of PETase by engineered Yarrowia lipolytica for efficient poly(ethylene terephthalate) biodegradation. Science of the Total Environment, 846, 157358.
- Kumartasli, S., & Avinc, O. (2020). Important step in sustainability: Polyethylene terephthalate recycling and the recent developments. In S. S. Muthu & M. A. Gardetti (Eds.), Sustainability in the Textile and Apparel Industries, (pp. 1–19). Springer. https://doi.org/10.1007/ 978-3-030-38013-7_1
- Liu, B., He, L., Wang, L., Li, T., Li, C., Liu, H., Luo, Y., & Bao, R. (2018). Protein crystallography and site-direct mutagenesis analysis of the poly(ethylene terephthalate) hydrolase PETase from Ideonella sakaiensis. ChemBioChem, 19, 1471–1475. https://onlinelibrary. wiley.com/doi/full/10.1002/cbic.201800097
- Loredo-Treviño, A., Gutiérrez-Sánchez, G., Rodríguez-Herrera, R., & Aguilar, C. N. (2012). Microbial enzymes involved in polyurethane biodegradation: A review. *Journal of Polymers and the Environment*, 20, 258–265. https://link.springer.com/article/10.1007/s10924-011-0390-5
- Lu, H., Diaz, D. J., Czarnecki, N. J., Zhu, C., Kim, W., Shroff, R., Acosta, D. J., Alexander, B. R., Cole, H. O., Zhang, Y., Lynd, N. A., Ellington, A. D., & Alper, H. S. (2022). Machine learning-aided engineering of hydrolases for PET depolymerization. *Nature*, 604, 662–667. https://www.nature.com/articles/s41586-022-04599-z
- Ma, Y., Yao, M., Li, B., Ding, M., He, B., Chen, S., Zhou, X., & Yuan, Y. (2018). Enhanced poly(ethylene terephthalate) hydrolase activity by protein engineering. *Engineering*, 4, 888–893.
- Musil, M., Stourac, J., Bendl, J., Brezovsky, J., Prokop, Z., Zendulka, J., Martinek, T., Bednar, D., & Damborsky, J. (2017). FireProt: Web server for automated design of thermostable proteins. *Nucleic Acids Research*, 45, W393–W399. https://academic.oup.com/nar/article/ 45/W1/W393/3760185
- Pasula, R. R., Lim, S., Ghadessy, F. J., & Sana, B. (2022). The influences of substrates' physical properties on enzymatic PET hydrolysis: Implications for PET hydrolase engineering. *Engineering Biology*, 6, 17–22. https://onlinelibrary.wiley.com/doi/full/10. 1049/enb2.12018

- Pirillo, V., Pollegioni, L., & Molla, G. (2021). Analytical methods for the investigation of enzyme-catalyzed degradation of polyethylene terephthalate. The FEBS Journal, 288, 4730–4745.
- Schrodinger LLC. (2021). The PyMOL Molecular Graphics System, Version 2.5.
- Schubert, S., Schaller, K., Bååth, J. A., Hunt, C., Borch, K., Jensen, K., Brask, J., & Westh, P. (2022). Reaction pathways for the enzymatic degradation of poly(ethylene terephthalate): What characterizes an efficient PET-hydrolase? *ChemBioChem*, e202200516. https://www.biorxiv.org/content/10.1101/2022.09.13.507771v1
- Seeley, M. E., Song, B., Passie, R., & Hale, R. C. (2020). Microplastics affect sedimentary microbial communities and nitrogen cycling. *Nature Communications*, 11, 2372. https://www.nature.com/articles/s41467-020-16235-3
- Seo, H., Kim, S., Son, H. F., Sagong, H.-Y., Joo, S., & Kim, K.-J. (2019). Production of extracellular PETase from Ideonella sakaiensis using sec-dependent signal peptides in *E. coli. Biochemical and Biophysical Research Communications*, 508, 250–255. https://linkinghub.elsevier.com/retrieve/pii/S0006291X18325117
- Shabbir, S., Faheem, M., Ali, N., Kerr, P. G., Wang, L. F., Kuppusamy, S., & Li, Y. (2020). Periphytic biofilm: An innovative approach for biodegradation of microplastics. Science of the Total Environment, 717, 137064.
- Shi, L., Liu, H., Gao, S., Weng, Y., & Zhu, L. (2021). Enhanced extracellular production of IsPETase in *Escherichia coli* via engineering of the pelb signal peptide. *Journal of Agricultural and Food Chemistry*, 69, 2245–2252. https://doi.org/10.1021/acs.jafc.0c07469. https://pubs.acs.org/doi/abs/
- Son, H. F., Cho, I. J., Joo, S., Seo, H., Sagong, H. Y., Choi, S. Y., Lee, S. Y., & Kim, K. J. (2019). Rational protein engineering of thermo-stable PETase from Ideonella sakaiensis for highly efficient PET degradation. ACS Catalysis, 9, 3519–3526. https://doi.org/10.1021/acscatal.9b00568. https://pubs.acs.org/doi/abs/
- Son, H. F., Joo, S., Seo, H., Sagong, H. Y., Lee, S. H., Hong, H., & Kim, K. J. (2020). Structural bioinformatics-based protein engineering of thermo-stable PETase from Ideonella sakaiensis. *Enzyme and Microbial Technology*, 141, 109656.
- De Souza Machado, A. A., Lau, C. W., Kloas, W., Bergmann, J., Bachelier, J. B., Faltin, E., Becker, R., Görlich, A. S., & Rillig, M. C. (2019). Microplastics can change soil properties and affect plant performance. Environmental Science & Technology, 53, 6044–6052. https://doi.org/10.1021/acs.est.9b01339. https://pubs.acs.org/doi/abs/
- De Souza MacHado, A. A., Lau, C. W., Till, J., Kloas, W., Lehmann, A., Becker, R., & Rillig, M. C. (2018). Impacts of microplastics on the soil biophysical environment. *Environmental Science & Technology*, 52, 9656–9665. https://doi.org/10.1021/acs.est.8b02212. https://pubs.acs.org/doi/abs/
- Studier, F. W. (2005). Protein production by auto-induction in highdensity shaking cultures. *Protein Expression and Purification*, 41, 207–234.
- Sumbalova, L., Stourac, J., Martinek, T., Bednar, D., & Damborsky, J. (2018). HotSpot Wizard 3.0: Web server for automated design of mutations and smart libraries based on sequence input information. *Nucleic Acids Research*, 46, W356–W362.
- Uheida, A., Mejía, H. G., Abdel-Rehim, M., Hamd, W., & Dutta, J. (2021). Visible light photocatalytic degradation of polypropylene microplastics

- in a continuous water flow system. *Journal of Hazardous Materials*, 406, 124299.
- Wong, J. K. H., Lee, K. K., Tang, K. H. D., & Yap, P. S. (2020). Microplastics in the freshwater and terrestrial environments: Prevalence, fates, impacts and sustainable solutions. *Science of the Total Environment*, 719, 137512.
- Woodley, J. M. (2013). Protein engineering of enzymes for process applications. *Current Opinion in Chemical Biology*, 17, 310–316. https://linkinghub.elsevier.com/retrieve/pii/S1367593113000513
- Wu, T., Yu, J., Gale-Day, Z., Woo, A., Suresh, A., Hornsby, M., & Gestwicki, J. E. (2020). Three essential resources to improve differential scanning fluorimetry (DSF) experiments. bioRxiv. https://www.biorxiv.org/content/10.1101/2020.03.22.002543v1
- Yang, S. S., Ding, M. Q., He, L., Zhang, C. H., Li, Q. X., Xing, D. F., Cao, G. L., Zhao, L., Ding, J., Ren, N. Q., & Wu, W. M. (2021). Biodegradation of polypropylene by yellow mealworms (*Tenebrio molitor*) and superworms (Zophobas atratus) via gut-microbe-dependent depolymerization. *Science of the Total Environment*, 756, 144087.
- Yoshida, S., Hiraga, K., Takehana, T., Taniguchi, I., Yamaji, H., Maeda, Y., Toyohara, K., Miyamoto, K., Kimura, Y., & Oda, K. (2016). A bacterium that degrades and assimilates poly(ethylene terephthalate). *Science*, 351, 1196–1199. https://doi.org/10.1126/science.aad6359. https://www.science.org/doi/abs/
- Zeng, W., Guo, L., Xu, S., Chen, J., & Zhou, J. (2020). High-throughput screening technology in industrial biotechnology. *Trends in Biotechnology*, 38, 888–906. https://doi.org/10.1016/j.tibtech.2020.01.001
- Zhang, G., Brokx, S., & Weiner, J. H. (2006). Extracellular accumulation of recombinant proteins fused to the carrier protein YebF in *Escherichia coli*. *Nature Biotechnology*, 24, 100–104.
- Zhang, K., Hamidian, A. H., Tubić, A., Zhang, Y., Fang, J. K. H., Wu, C., & Lam, P. K. S. (2021). Understanding plastic degradation and microplastic formation in the environment: A review. *Environmental Pollution*, 274, 116554.
- Zhong-Johnson, E. Z. L., Voigt, C. A., & Sinskey, A. J. (2021). An absorbance method for analysis of enzymatic degradation kinetics of poly(ethylene terephthalate) films. *Scientific Reports*, 11, 1–9. https://www.nature.com/articles/s41598-020-79031-5
- Zhou, D., Chen, J., Wu, J., Yang, J., & Wang, H. (2021). Biodegradation and catalytic-chemical degradation strategies to mitigate microplastic pollution. Sustainable Materials and Technologies, 28, e00251.
- Zurier, H. S., & Goddard, J. M. (2021). Biodegradation of microplastics in food and agriculture. Current Opinion in Food Science, 37, 37-44. https://linkinghub.elsevier.com/retrieve/pii/S2214799320300680

SUPPORTING INFORMATION

Additional supporting information can be found online in the Supporting Information section at the end of this article.

How to cite this article: Zurier, H. S., & Goddard, J. M. (2023). A high-throughput expression and screening platform for applications-driven PETase engineering. *Biotechnology and Bioengineering*, 1–15. https://doi.org/10.1002/bit.28319